CANCER

Circadian disruption promotes tumor-immune microenvironment remodeling favoring tumor cell proliferation

I. Aiello[1,2]*, M. L. Mul Fedele[1]*, F. Román[1], L. Marpegan[1], C. Caldart[1], J. J. Chiesa[1], D. A. Golombek[1†], C. V. Finkielstein[2†], N. Paladino[1]

Circadian disruption negatively affects physiology, posing a global health threat that manifests in proliferative, metabolic, and immune diseases, among others. Because outputs of the circadian clock regulate daily fluctuations in the immune response, we determined whether circadian disruption results in tumor-associated immune cell remodeling, facilitating tumor growth. Our findings show that tumor growth rate increased and latency decreased under circadian disruption conditions compared to normal light-dark (LD) schedules in a murine melanoma model. Circadian disruption induced the loss or inversion of daily patterns of M1 (proinflammatory) and M2 (anti-inflammatory) macrophages and cytokine levels in spleen and tumor tissues. Circadian disruption also induced (i) deregulation of rhythmic expression of clock genes and (ii) of cyclin genes in the liver, (iii) increased *CcnA2* levels in the tumor, and (iv) dampened expression of the cell cycle inhibitor $p21^{WAF/CIP1}$, all of which contribute to a proliferative phenotype.

INTRODUCTION

The circadian clock is responsible for the generation and entrainment of rhythms for almost all physiological and behavioral functions of the body (e.g., body temperature, hormonal secretion, sleep, and locomotor activity), enabling adaptation to cyclic environmental changes. The molecular mechanism of the circadian clock arises from negative transcriptional feedback, which generates oscillations with periods close to 24 hours. In mammals, the core loop includes the positive elements Clock and Bmal1, inducing the expression of the negative elements Per1 to Per3 and Cry1 and Cry2, which, in turn, repress the transcriptional activity of the positive elements in a process where compartmentalization, shuttling, and posttranslational events determine the pace of the circadian clock (*1*). This cell-autonomous pacemaker mechanism has been found in almost every cell in the body. The main biological clock resides in the hypothalamic suprachiasmatic nuclei (SCN), and the principal environmental signal that adjusts its activity is the light-dark (LD) cycle. In turn, the SCN controls circadian oscillators in peripheral tissues (e.g., liver, lung, and other brain areas) through neural, hormonal, and behavioral pathways to maintain an optimal phase relation between them and with the environment (*2*).

In mammals, shifting the activity period to an atypical time of the day (e.g., by shift work or jet lag in humans) causes a temporal misalignment that, under chronic conditions, might result in disease onset (e.g., cardiometabolic syndromes, obesity, and cancer) and physical and mental health disorders. Whereas these findings were initially brought to our attention by epidemiological studies, the use of animal models has been pivotal to uncovering the genetic and environmental links that, when compromised by circadian disruption, lead to disease onset [reviewed in (*3*)]. A case in point was the initial finding that tumor-bearing mice increased their tumor growth rate when exposed to experimental chronic jet lag (CJL), constant light (LL), or other alterations of the molecular circadian clock (*3*). Whole genome-wide transcript profiling showed that ~10% of the cell transcriptome, including genes involved in cell cycle transition, response to DNA damage, and cell death processes, were under circadian control [reviewed in (*4*)], all of which suggest a relevant role for clock components in establishing proliferative disorders.

The development of cancer and its response to therapeutic protocols are strongly influenced by innate and adaptive immune systems, which either promote or attenuate tumorigenesis. As the circadian clock modulates several immune parameters including the number of different cell types (e.g., macrophages and $CD4^+$ and $CD8^+$ T cells) in different tissues (e.g., peripheral blood and spleen), daily cytokine fluctuations, phagocytic activity, and response to the immune challenge (e.g., lipopolysaccharide) [reviewed in (*5*)], its derangement deregulates the inflammatory processes that are predicted to favor establishment and progression of tumors (*6*). Specifically, macrophages can differentiate into two functional profiles, M1 and M2. The M1 phenotype is more closely associated with inflammatory antitumor immunity, whereas the M2 phenotype, a more functionally diverse subset of macrophages, exhibits immunosuppressive and homeostatic functions (*7*). Chronic inflammation can promote tumor development and progression; nevertheless, the balance between the activation of immunological tolerance and inflammatory pathways is certainly relevant to tumor immunity. Tumor-specific or tumor-associated antigens can activate antitumor immune responses by dendritic cells (DCs) and M1 macrophage–mediated activation of cytotoxic T lymphocytes and natural killer (NK) cells. In addition, induction of tolerance can be achieved by recruitment to the tumor microenvironment and differentiation of immunosuppressive cells such as M2 macrophages, myeloid-derived suppressor cells (MDSCs), tumor-associated neutrophils, and regulatory T cells (T_{regs}) [reviewed in (*8*)].

The aim of this study was to analyze the impact of chronic circadian derangement in tumor-immune microenvironment remodeling and tumor growth in a nonmetastatic melanoma mouse model.

[1]Laboratorio de Cronobiología, Universidad Nacional de Quilmes, Buenos Aires, Argentina. [2]Integrated Cellular Responses Laboratory, Department of Biological Sciences, Fralin Life Sciences Institute, Virginia Tech, Blacksburg, VA, USA.
*These authors contributed equally to this work.
†Corresponding author. Email: dgolombek@unq.edu.ar (D.A.G.); finkielc@vt.edu (C.V.F.)

RESULTS

Circadian disruption promotes tumor growth

To understand the effect of a circadian disruption protocol on the rate of tumor growth, mice were maintained under an experimental LD (LD12:12) or CJL schedule [6-hour advance of the LD12:12 cycle every 2 days (*9*)] for 3 weeks before they were subcutaneously challenged with B16F0 nonmetastatic melanoma cells. Following inoculation, animals were maintained under each experimental light schedule, i.e., LD or CJL, until reaching the end point of the tumor protocol as defined in Materials and Methods. We chose to work with B16F0 cells because their tumor growth rate in vivo is modulated by the immune system (*10*).

First, we recapitulated the circadian disruption tumor growth model in vivo in CJL-treated mice and compared tumor growth to matching points in mice maintained under LD conditions. Tumor size under circadian desynchronization increased significantly compared to those grown under LD conditions ($P < 0.01$; Fig. 1A). Moreover, the survival curve was significantly different between the CJL and LD mice groups ($P = 0.0153$; Fig. 1B). In addition, tumor latency, measured as the elapsed time between the injection of B16F0 cells and the moment a palpable tumor was detectable in the animal (vol.^{t} ~ 1 mm^3), was 15 ± 0.85 days after inoculation in CJL versus 25.8 ± 3.64 days in LD treated-animals ($P = 0.037$; Fig. 1C).

We then determined whether alterations in the light schedule influenced tumor vasculogenesis. We found that, whereas the number of blood vessels around the site of tumor cell inoculation (1 week after injection) remained comparable between both circadian protocols (fig. S1, A and B), the number of intratumor blood vessels (vol.^{t} of 2000 to 2500 mm^3) increased significantly under CJL conditions ($P = 0.0007$; fig. S1, C and D).

Circadian desynchronization promotes tumor-immune microenvironment remodeling

Because the composition of the tumor-immune microenvironment influences tumor growth and shapes therapeutic treatments (*11*), we determined whether circadian disruption could influence the proportion of various immune cells in the tumor microenvironment and, in turn, favor tumor progression. Accordingly, we first examined the percentage of different tumor-infiltrating leukocytes in tumor samples collected over a 24-hour period [Zeitgeber time 3 (ZT3), ZT9, ZT15, and ZT21] from animals maintained in either constant LD or chronic circadian disruption (CJL) schedules (Fig. 2 and fig. S2). Because there were no significant differences between data obtained in ZT3 and ZT9 or between ZT15 and ZT21, we grouped the values obtained during the day (ZT3 and ZT9) and night (ZT15 and ZT21) and summarized them as diurnal and nocturnal data, respectively (table S1).

We evaluated the percentage of total macrophages within tumor samples and did not observe significant differences between time points [LD: ZT3: 52.2 ± 8.97%, ZT9: 51.48 ± 8.34%, ZT15: 55.16 ± 4.08%, ZT21: 31.08 ± 6.83%; CJL: ZT3: 56.32 ± 5.08%, ZT9: 47.04%, ZT15: 28.2 ± 8.46%, ZT21: 28.08 ± 9.98%; P = n.s. (not significant); table S1]. However, our results show several remarkable changes in M1 and M2 macrophage levels between the two experimental conditions (Fig. 2). Under LD exposure, M1 macrophages exhibited a nearly twofold increase in their levels at ZT15 and ZT21 compared to ZT9 ($P < 0.05$; Fig. 2A), while in animals exposed to CJL this difference was inverted, showing higher levels at ZT9 ($P < 0.05$; Fig. 2A). Despite the lack of significant differences between time points in the levels of M2 cells (Fig. 2B), we found interesting results when comparing diurnal versus nocturnal levels. Under LD exposure, M1 and M2 macrophage levels were in antiphase, with an increase in the level of M1 cells during the night (LD Day versus LD Night: $P = 0.004$; table S1) and a comparable reduction of M2 cells in this phase (LD Day versus LD Night: $P = 0.003$; table S1). The distribution of M1 and M2 cells in tumors from animals exposed to CJL exhibited a sharp contrast with that of LD animals (table S1). Whereas chronic circadian disruption reversed and dampened the levels of M1-infiltrated cells in the tumor (CJL Day versus CJL Night: $P = 0.049$; LD Night versus CJL Night: $P = 0.0004$; table S1), the levels of M2 macrophages lost their day-night differences and remained constant throughout the whole cycle (CJL Day versus CJL Night: P = n.s., LD Day versus CJL Day: $P = 0.017$; table S1). These results indicate that circadian disruption induces important changes in the composition of the tumor-infiltrated immune cells at different times of the day.

Because M1 and M2 cells have opposite functions and can inhibit one another, the M1/M2 ratio has a predictive value on tumor growth (*12*). Although we did not observe substantial differences among time points (Fig. 2C), tumors from animals under LD exhibited a ratio that favored M1-mediated immunostimulation and tumor suppressor activity during the night and a more tumor-prone phenotype characterized by M2-mediated immune suppression during the day (LD Day versus LD Night: $P = 0.0028$; table S1). These temporal differences in infiltration were blunted in CJL animals, favoring a phenotype in which tumor progression is

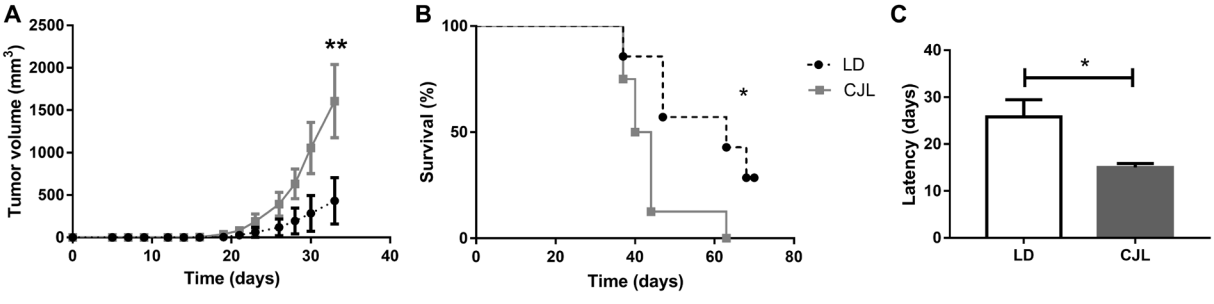

Fig. 1. Characterization of tumor growth and animal survival under CJL schedules. Mean ± SEM of tumor size (**A**), survival (**B**), and tumor latency (**C**) in C57BL/6J mice under LD and CJL conditions injected subcutaneously with 30,000 cells of the murine melanoma cell line B16F0. Tumor latency: day of tumor detection by palpation (approximately 1 mm^3). (A) Repeated-measures ANOVA interaction time × light schedule, $P < 0.0001$, post hoc test: day 33: CJL: 1607.5 ± 431.7 mm^3, LD: 432.7 ± 272.9 mm^3, $^{**}P < 0.01$; (B) survival [log-rank (Mantel-Cox)] test: $^{**}P = 0.0153$; (C) *t* test: $^{*}P = 0.037$; $n = 14$ per condition.

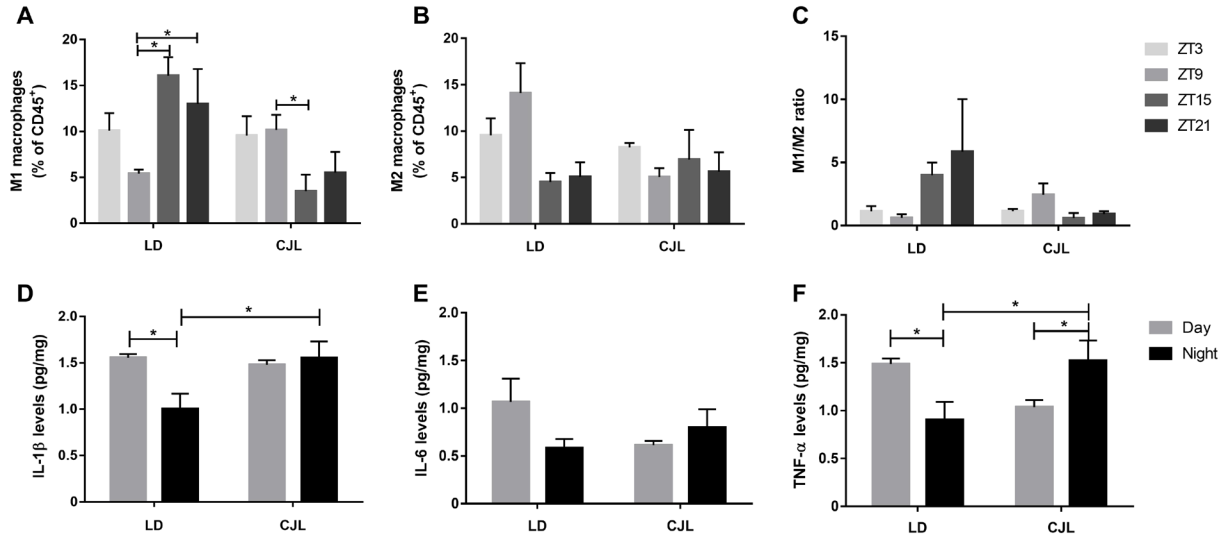

Fig. 2. Daily pattern of immune parameters in tumor under CJL conditions. Mean ± SEM of the percentage of M1 (**A**) and M2 (**B**) macrophages, and the M1/M2 ratio (**C**) in tumor samples detected by flow cytometry taken at ZT3, ZT9, ZT15, and ZT21 as described in fig. S4, and mean ± SEM of protein levels of IL-1β (**D**), IL-6 (**E**), and TNF-α (**F**) in tumor tissue samples taken at ZT6 and ZT18 (day and night, respectively) measured by ELISA. (A) Kruskal Wallis test: $P = 0.028$, LD: ZT3: 10.09 ± 1.90%, ZT9: 5.41 ± 0.43%, ZT15: 16.07 ± 2.0%, ZT21: 12.99 ± 3.80%; CJL: ZT3: 9.55 ± 2.12%, ZT9: 10.15 ± 1.65%, ZT15: 3.49 ± 1.79%, ZT21: 5.51 ± 2.26; post hoc test: $^*P < 0.05$. (D) Two-way ANOVA: interaction time × light schedule: $P = 0.038$, LD Day: 1.55 ± 0.04 pg/mg, LD Night: 1.03 ± 016 pg/mg, CJL Day: 1.48 ± 0.04 pg/mg, CJL Night: 1.55 ± 0.18 pg/mg; post hoc test: $^*P = 0.019$ for LD Day versus LD Night, and $^*P = 0.027$ for LD Night versus CJL Night. (F) Two-way ANOVA: interaction time × light schedule: $P = 0.0067$, LD Day: 1.48 ± 0.06 pg/mg, LD Night: 0.90 ± 0.19 pg/mg, CJL Day: 1.03 ± 0.06 pg/mg, CJL Night: 1.52 ± 0.21 pg/mg, post hoc test: $^*P = 0.03$ for LD Day versus LD Night, $^*P = 0.04$ for CJL Day versus CJL Night, and $^*P = 0.038$ for LD Night versus CJL Night. $n = 3$ to 4 per condition and time point.

likely favored at all times (LD Night versus CJL Night: $P = 0.0038$; table S1).

Together, the data obtained for the M1 and M2 macrophages suggest that (i) under normal LD conditions, there is a daily pattern in the levels of M1 and M2 cells in the tumor, which translates into daily variations in the M1/M2 ratio, with the antitumor immunity being favored during the night, and (ii) circadian disruption not only induces the loss of these daily patterns but also decreases the M1/M2 ratio, which could facilitate the tumor growth.

In this context, we chose to evaluate the levels of proinflammatory cytokines interleukin-1β and interleukin-6 (IL-1β and IL-6) and tumor necrosis factor–α (TNF-α; Fig. 2, D to F). Circadian oscillation of the mentioned cytokines was previously observed in macrophages in vitro (*13*–*15*). Intratumor levels of IL-1β and IL-6 switched from a daily cycle variation under LD conditions to a largely invariant level under CJL (IL-1β: LD Day versus LD Night: $P = 0.019$ and LD Night versus CJL Night: $P = 0.027$; Fig. 2, D and E). Unlike interleukins, TNF-α also maintained distinct expression levels in a daily cycle within the tumor but appeared to be in antiphase in samples from animals treated under LD and CJL conditions (LD Day versus LD Night: $P = 0.03$, CJL Day versus CJL Night: $P = 0.04$, LD Night versus CJL Night: $P = 0.038$; Fig. 2F).

The outcome of tumor growth is tightly linked to the balance among infiltrating leukocytes with antagonistic functions, which constitutes the tumor-immune microenvironment [reviewed in (*8*)]. To obtain a more accurate representation of the changes in intratumor leukocyte populations in animals subjected to circadian disruption, we also analyzed the total leukocyte ($CD45^+$ cells) percentage and its composition (i.e., T_{regs} and MDSCs; fig. S2 and table S1). Our results indicate that tumor samples from animals maintained under the CJL schedule have higher levels of leukocytes than animals subjected to LD conditions (LD versus CJL: $P = 0.01$; table S1), without time-dependent differences in accumulation (LD Day versus LD Night: P = n.s.; CJL Day: versus CJL Night: P = n.s.; table S1 and fig. S2A). Accordingly, total T helper lymphocytes ($CD4^+$) showed a modest, yet substantial intratumor accumulation, which was larger in CJL-treated animals than in LD-treated animals (LD versus CJL: $P = 0.038$; table S1) and remained unaltered over the different time points (LD Day versus LD Night: P = n.s., CJL Day versus CJL Night: P = n.s.; table S1 and fig. S2B). T regulatory $CD4^+$ lymphocytes and MDSC accumulation among treatments were not significantly different, although increased intratumor levels of these cells are usually associated with higher tumor grade and poorer prognosis in some cancers [fig. S2, C and D, and table S1 (*8*)].

Overall, our results favor a model in which circadian disruption modifies the immune microenvironment, which, in turn, could facilitate tumor growth. The decrease in the M1/M2 ratio observed during the night in tumors of mice under CJL would tilt the balance toward a more tolerogenic immune profile, which promotes tumor progression.

Circadian deregulation and tumor growth alter macrophage distribution in peripheral organs

To evaluate the impact of circadian desynchronization on the immune system, we analyzed the temporal distribution of immune cells in the spleen of control animals (without tumor; Fig. 3, A to E). We reasoned that alterations in the peripheral immune response could be related to the shorter tumoral latency observed in mice under CJL conditions. In addition, because the presence of the tumor can influence the immune response, we also assessed the combined effect of tumor presence and circadian desynchronization on spleen immune cells.

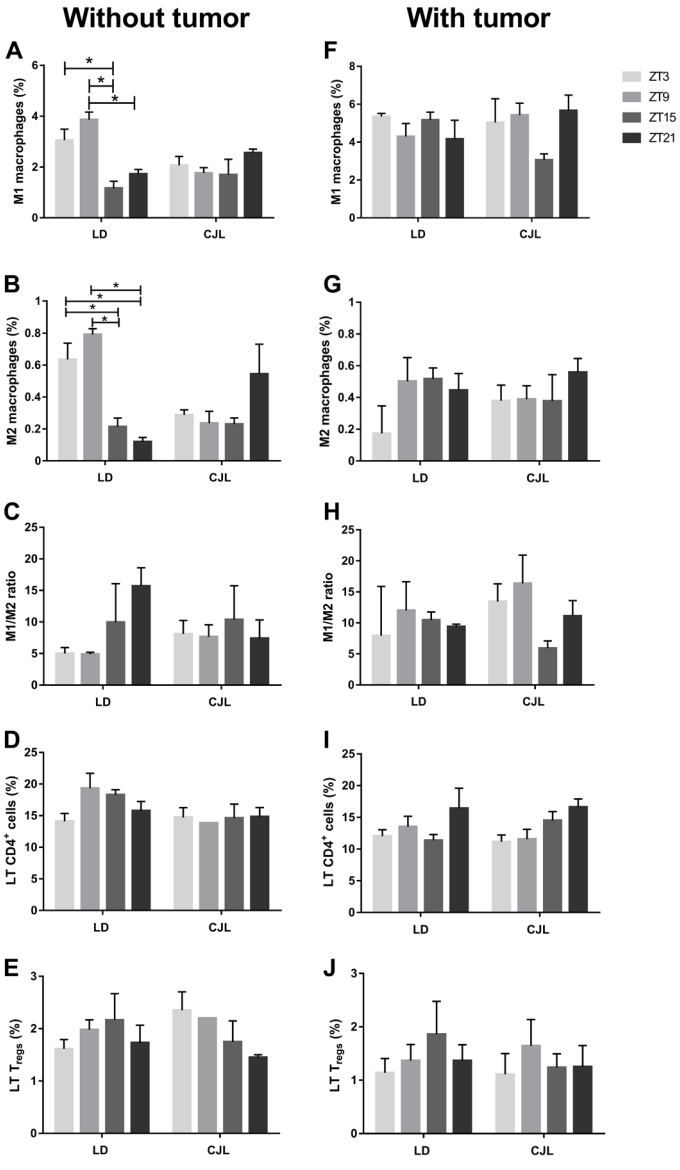

Fig. 3. Daily pattern of immune cells in spleen tissue of mice carrying tumors under CJL conditions. Mean ± SEM of the percentage of M1 (**A** and **F**) and M2 (**B** and **G**) macrophages, M1/M2 ratio (**C** and **H**), LT CD4$^+$ (**D** and **I**), and LT T_{reg} (**E** and **J**), detected by flow cytometry, in spleen tissue of control mice (A to D) or tumor-bearing mice (E to I) maintained under an LD or CJL schedule. (A) Kruskal-Wallis test: $P = 0.01$, LD: ZT3: 3.05 ± 0.43%, ZT9: 3.85 ± 0.29%, ZT15: 1.16 ± 0.27%, ZT21: 1.72 ± 0.18%; CJL: ZT3: 2.06 ± 0.34%, ZT9: 1.76 ± 0.20%, ZT15: 1.69 ± 0.60%, ZT21: 2.55 ± 0.14%. (B) Kruskal-Wallis test: $P = 0.017$; LD: ZT3: 0.63 ± 0.12%, ZT9: 0.79 ± 0.03%, ZT15: 0.21 ± 0.05%, ZT21: 0.12 ± 0.03%; CJL: ZT3: 0.17 ± 0.17%, ZT9: 0.50 ± 0.15%, ZT15: 0.51 ± 0.06%, ZT21: 0.44 ± 0.10%. For (C to H) Kruskal-Wallis test: P = n.s.; post hoc test: *$P < 0.05$. $n = 3$ to 4 per condition and time point.

We first addressed whether the distribution of spleen M1 and M2 macrophages was influenced by changes in circadian synchronization (Fig. 3, A to C, and table S1). Thereby, in animals without tumor, our results showed an increased level at ZT3 and ZT9 for both M1 and M2 cells compared to ZT15 and ZT21 (M1: $P < 0.05$ for ZT3 versus ZT15 and ZT9 versus ZT15 and ZT21; M2: $P < 0.05$ for ZT3 and ZT9 versus ZT15 and ZT21; Fig. 3, A and B, respectively). Moreover, these results were consistent with a daily pattern of M1 and M2 percentages in this tissue, with higher levels during the day for both types of cells (without tumor: M1: LD Day versus LD Night: $P = 0.000016$; M2: LD Day versus LD Night: $P = 0.000038$; table S1). Circadian desynchronization was sufficient to suppress LD patterns of M1 and M2 levels in the spleen, which, per se, could be a contributing factor favoring early stages of tumor development (M1 and M2: P = n.s. for all comparisons; Fig. 3, A and B, respectively). Moreover, when we compared the daily pattern from LD with CJL, we found a decrease in M1 diurnal levels under CJL conditions (M1: CJL Day versus CJL Night: P = n.s., LD Day versus CJL Day: $P = 0.001$; table S1), which was not compensated for during the night as was observed for M2 cells (M2: CJL Day versus CJL Night: P = n.s.; LD Day versus CJL Day: $P = 0.0005$; LD Night versus CJL Night: $P = 0.049$; table S1). However, we did not find significant differences in the M1/M2 ratio between these samples (M1/M2: P = n.s. for all comparisons; Fig. 3C and table S1).

Next, we evaluated the effect that tumor growth had on macrophage distribution in the host spleen under LD and CJL conditions (with tumor; Fig. 3, F to J). Our results showed that the sole presence of the tumor was sufficient to influence the polarization of macrophages under LD conditions compared to sham animals. For both M1 and M2 cell types, the daily pattern was abolished, with maximum levels at all time points (LD: M1 and M2: P = n.s. for all comparisons; Fig. 3, F and G, and table S1). In tumor-bearing animals under CJL, the levels of M1 and M2 cells were similar to those under LD, suggesting that the impact of the presence of the tumor is more relevant than the circadian effect (CJL: M1 and M2: P = n.s. for all comparisons; Fig. 3, F and G, and table S1). As expected, we did not find any significant difference in the M1/M2 ratio between these groups (M1/M2: P = n.s. for all comparisons; Fig. 3H and table S1).

In addition, the percentage of total LT CD4$^+$ and T_{regs} in spleen did not present daily differences and their levels were similar between both light schedules and in animals with or without tumors (Fig. 3, D, E, I, and J, and table S2), suggesting that these variables do not participate in the increased tumor growth rate observed in desynchronized mice. Together, our results emphasize a connection between components of the tumor microenvironment, particularly macrophages, and circadian variables that are altered in peripheral tissues under chronic circadian desynchronization. Thus, we speculate that circadian desynchronization in peripheral organs, e.g., spleen, resulting from a CJL schedule would favor the early stages of tumor development.

Circadian disruption alters the expression pattern of clock genes in the liver

To gain a deeper understanding of the contribution of host and tumor clocks to the rate of abnormal tumor growth, we monitored the oscillatory expression of the core clock genes *Bmal1* and *Cry1* using real-time polymerase chain reaction (PCR) in liver samples obtained from mice maintained under LD or CJL schedules (Fig. 4). As expected, the mRNA levels of *Bmal1* and *Cry1* exhibited a rhythmic expression pattern in the liver of animals maintained under constant LD conditions and in the absence of tumors [cosinor: *Bmal1*: $P = 0.006$, acrophase = 23.59 hours; *Cry1*: $P = 0.024$, acrophase = 21.23 hours; Fig. 4, A and B, and table S2 (*16*)]. When similar studies were carried out in sham animals exposed to a CJL schedule, the oscillation of *Bmal1* and *Cry1* genes, measured by the cosinor method,

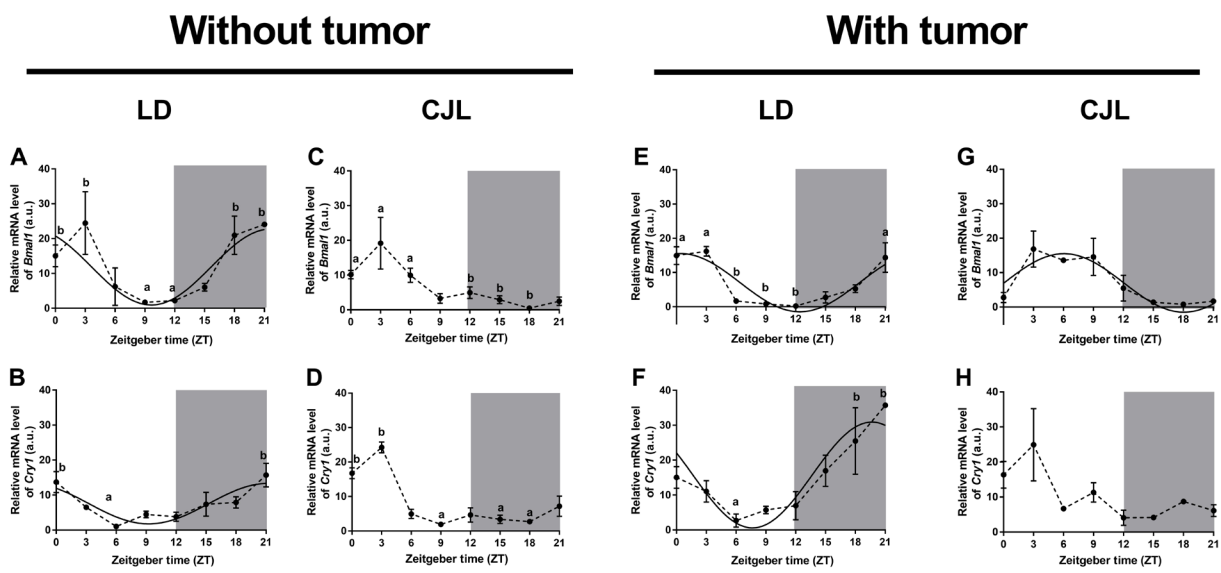

Fig. 4. Rhythms of clock genes in liver under the CJL schedule. Mean ± SEM of relative mRNA levels of *Bmal1* (**A**, **C**, **E**, and **G**) and *Cry1* (**B**, **D**, **F**, and **H**) in the livers of mice carrying tumors (E to H) or controls (A to D), under LD (A, B, E and F) and CJL (C, D, G, and H) conditions detected by real-time PCR in eight time points (ZT0, ZT3, ZT6, ZT9, ZT12, ZT15, ZT18, and ZT21). Curves plotted over the data (A, B, and E to G) correspond to cosinor analysis adjusted to 24 hours. Only the statistically significant cosinor analyses were plotted (table S2). Nonparametric Kruskal-Wallis test: (A) $P = 0.001$, (B) $P = 0.002$, (C) $P = 0.007$, (D) $P = 0.016$, (E) $P = 0.016$, and (F) $P = 0.048$; post hoc test: $P < 0.05$: a versus b. $n = 3$ to 4 per condition and time point. a.u., arbitrary units.

was deemed not significant (Fig. 4, C and D, and table S2). Nevertheless, analysis of variance (ANOVA) analyses showed marginal, yet significant, daily differences of mRNA expression for *Bmal1* and *Cry1* that peaked during the day. These results suggest that the liver circadian clock is altered but not completely abrogated. In this context, CJL might cause a phase advance in the rhythmic expression of clock genes that peak at ZT3, 3 and 6 hours later than the acrophases for *Bmal1* and *Cry1* observed under LD conditions, respectively (23.59 and 21.23 hours).

Next, we determined whether animals bearing tumors exhibit a distinct circadian phenotype in their peripheral liver clock. Whereas the pattern of clock gene expression remained largely similar to control animals (without tumor) maintained under a normal photoperiod (cosinor: *Bmal1*: $P = 0.028$, acrophase = 22.85 hours; *Cry1*: $P = 0.006$, acrophase = 19.68 hours; Fig. 4, E and F, and table S2), those exposed to a CJL schedule showed, again, relevant differences compared to control mice (Fig. 4, G and H, and table S2). These results suggest that the changes observed in clock gene expression in the liver are mainly the result of changes in the circadian schedule and that the presence of the tumor does not play a substantial role in such alterations.

The oscillations of *Bmal1* and *Cry1* are abrogated in the tumor tissue

Clock function was then monitored in tumoral tissue extracted at different times from animals maintained under different light schedules (fig. S3). The expression of *Bmal1* and *Cry1* genes did not show a rhythmic pattern under either an LD or CJL schedule (fig. S3, A to D). The lack of rhythmic patterns in these genes could be associated with a difference in the phase of the rhythms in each individual cell. However, the absence of differences between LD and CJL samples suggests that the expression of the clock genes *Bmal1* and *Cry1* in the tumor itself may not be implied in the increased growth rate under desynchronized conditions but could instead be related to deregulation of time-dependent gene expression in tumoral cells.

Cell cycle progression is compromised in hepatocytes exposed to chronic circadian disruption

Differentiated mammalian hepatocytes have the unique ability to exit quiescence and reenter the cell cycle as a result of physical (e.g., partial resection) or mitogenic stimuli, for which the presence of proinflammatory cytokines remains a required priming event (*17*). TNF-α and IL-6, two of the cytokines we found to be deregulated in tumor-bearing CJL-treated animals, are among the ligands favoring G_0-G_1 transition and are required for the establishment of early G_1 in vivo during liver regeneration (*18*). As a result, we first determined whether alterations in the immune makeup of animals exposed to circadian disruption translate into hepatocyte cell cycle remodeling in vivo and then evaluated whether the observed phenotype was altered in tumor-bearing animals (Fig. 5).

Initially, mice were exposed to LD or CJL light schedules, the liver tissue was excised at different time points, and markers for cell cycle progression were assessed. We chose to monitor mRNA levels of G_1-S and G_2-M cyclins and of the cyclin/cyclin-dependent kinase (Cdk) inhibitor $p21^{WAF/CIP1}$ (*Cdkn1a*) as these markers have been extensively characterized and represent entry into and progression through the cell cycle. In agreement with the in vivo quiescent nature of hepatocytes, the gene expression profile of *CcnE1*, *CcnA2*, and *CcnB1* (which encode for cyclins E, A2, and B1, respectively) exhibited low levels of expression in liver samples from animals exposed to a normal LD schedule (Fig. 5, A to C). Our results suggest that some hepatocytes might progress from quiescence to early G_1, as evidenced by a modest, yet significant, rise and progressive decline in the *CcnE1* level detected within the ZT9 and ZT15 window in LD samples (LD: ZT9 versus ZT18: $P < 0.05$; Fig. 5A). A basal level of *CcnA2* expression was identified, overlapping with *CcnE1* at

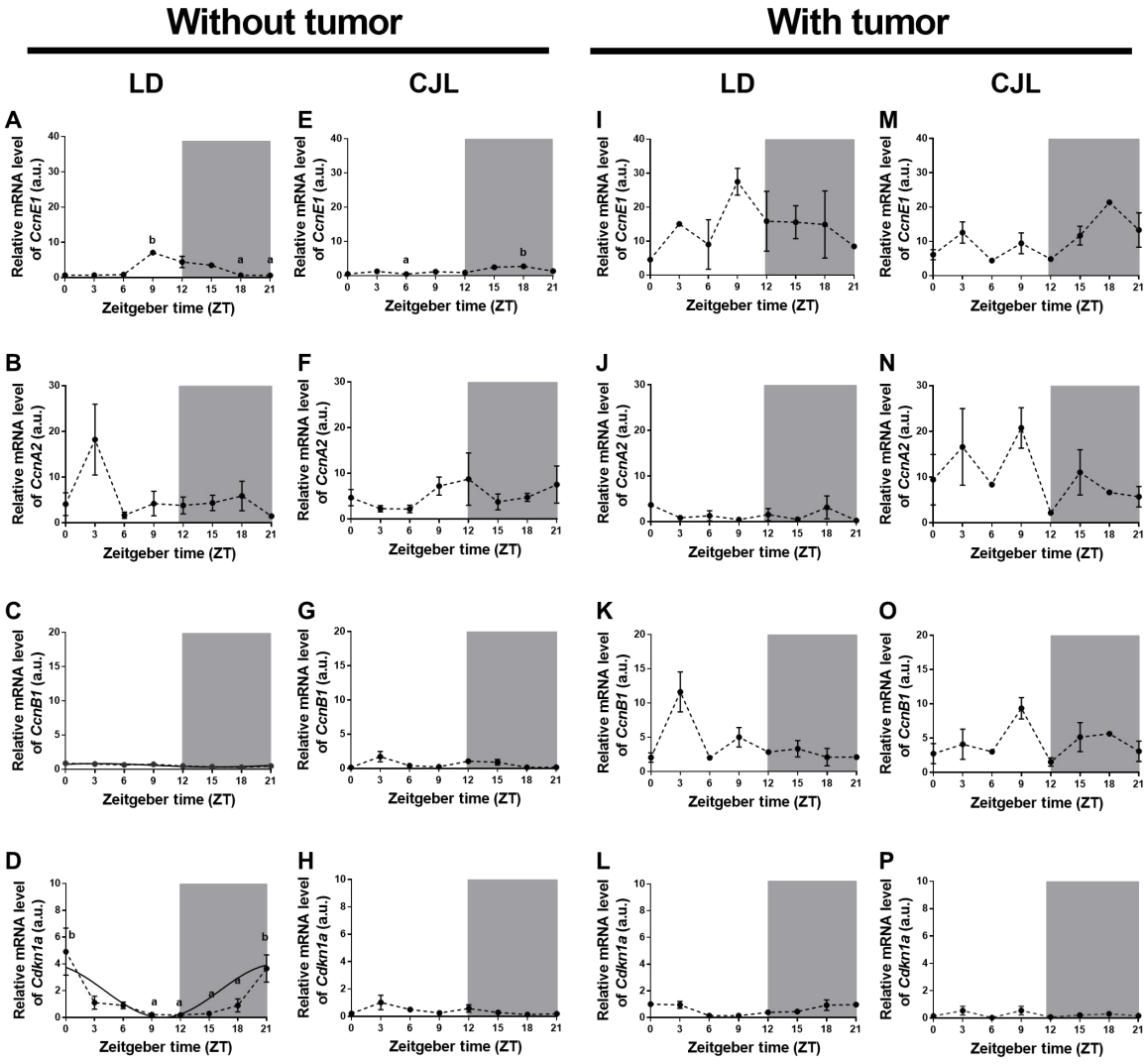

Fig. 5. Rhythms of cell cycle–related molecules in liver under a CJL schedule. Mean ± SEM of relative mRNA levels of the *CcnE1* (**A**, **E**, **I**, and **M**), *CcnA2* (**B**, **F**, **J**, and **N**), and *CcnB1* (**C**, **G**, **K**, and **O**) and the inhibitor $p21^{WAF/CIP1}$ (*Cdkn1a*; **D**, **H**, **L**, and **P**) in liver tissues of control mice (A to H) or mice carrying tumors (I to P), under LD (A to D and I to L) or CJL (E to H and M to P) conditions, detected by real-time PCR in eight time points (ZT0, ZT3, ZT6, ZT9, ZT12, ZT15, ZT18, and ZT21). Curves plotted over the data (C and D) that correspond to the cosinor analysis were adjusted to 24 hours. Only statistically significant cosinors were plotted (table S2). Kruskal-Wallis test: (A) $P = 0.011$, (D) $P = 0.012$, and (E) $P = 0.0023$; post hoc test: $P < 0.05$: a versus b: $n = 3$ to 4 per condition and time point.

ZT9 to ZT15 (Fig. 5B); thus, our results support a model in which cells become arrested at a restriction point located in mid-late G_1. This assumption is supported by the observation that $p21^{WAF/CIP1}$ accumulation occurred within the same time frame than the expression of G_1-S cyclins (cosinor: $P = 0.04$; Fig. 5D and table S2) and that the level of *CcnB1* remained low and invariable at all times (Fig. 5C).

The effect of the CJL schedule in the expression of cell cycle components was particularly noticeable when monitoring the mRNA profile of $p21^{WAF/CIP1}$ in liver samples (Fig. 5H). Figure 5 shows that the cyclin/Cdk inhibitor level (*Cdkn1a*) remained steady and low at all times under the CJL condition compared to LD (Fig. 5, D versus H). In addition, the profile of G_1-S cyclins was perturbed under a CJL schedule (Fig. 5, E to G) as reflected by the peak of maximum expression of cyclin E1 being shifted when compared to LD (i.e., *CcnE1*; Fig. 5, A versus E). Overall, these data suggest that the liver tissue from animals subjected to a CJL schedule exhibits perturbation at the cellular level, which could make the hepatocytes entirely competent to mitogenic and inflammatory signals.

We then determined whether the presence of a nonmetastatic tumor alters the molecular makeup of the liver favoring a proliferative state when animals were subjected to distinct light schedules. As shown in Fig. 5 (I to L), the sole presence of the tumor led to *CcnE1* up-regulation (by comparing the confidence interval of the mesor in table S2 and Fig. 5, A versus I) and $p21^{WAF/CIP1}$ dampening (cosinor: P = n.s.; table S1 and Fig. 5, D versus L) under LD conditions, suggesting that progression to late G_1 was favored. However, most cells likely remained uncommitted to DNA replication due to the lack of *CcnA2* expression (Fig. 5J).

The liver proliferative phenotype was enhanced in the presence of a tumor and under conditions of CJL (confidence interval of the mesor in table S2 for *CcnE1*: LD without tumor versus CJL with tumor, *CcnA2*: LD with tumor versus CJL with tumor, *CcnB1*: LD without

tumor versus CJL with tumor, *Cdkn1a*: LD with tumor versus CJL with tumor; table S2 and Fig. 5, M to P). Accordingly, both G_1-S and G_2-M cyclins showed an enhanced, cascade-like (*CcnE1*, *CcnA2*, and *CcnB1*; Fig. 5, N to P) expression of *CcnE1*, which was detected in early and late G_1 and before S-phase entry (Fig. 5M), whereas detectable levels of *CcnA2* and *CcnB1* were observed before or during G_2-M transitions (Fig. 5, N and O). We speculate that the enhanced proliferative phenotype observed in the liver tissue of tumor-bearing animals might have been facilitated by the accumulation of proinflammatory cytokines that made the hepatocytes competent to mitogenic signals.

Circadian modulation of cell cycle gene expression in tumor

Last, we evaluated whether chronic circadian deregulation affects the expression of cell cycle components in the tumor or, instead, disrupts their daily oscillation. Accordingly, tumor samples from animals maintained in either LD or CJL schedules were collected at different times and their expression was monitored by real-time quantitative reverse transcription PCR (Fig. 6). In agreement with the cell proliferative status within the tumor, mRNA expression of $p21^{WAF/CIP1}$ (*Cdkn1a*) remained at low levels throughout the time course analyzed (Fig. 6, A and B). Whereas exposure to CJL has a negligible effect on the expression and oscillation of the cyclin E1 and B1 transcripts (Fig. 6, C to E and I to K), both remained detectable and largely steady at all times; the expression of *CcnA2* exhibited a sustained increase (Fig. 6, F versus G: ZT9 to ZT15; Fig. 6H). These results suggest that, in addition to promoting tumor proliferation by developing a favorable immune niche, chronic disruption favors the up-regulation of key regulatory components, such as *CcnA2*, which favors cell cycle transitions.

DISCUSSION

The CJL protocol used in this work, 6-hour advances of the LD cycle every 2 days, generates an internal circadian desynchronization in which animals fail to entrain to the environmental cycle (*9*). Our results show and confirm an increased rate of tumor growth in mice under circadian disruption. Here, we first confirm data previously reported using different carcinogenesis models and light schedules of circadian disruption [CJL and constant light (*6*, *19*–*24*)]. Moreover, mice carrying mutations of clock genes (*22*, *25*) or those whose SCN was ablated (*26*) also showed an increased rate of tumoral growth. In addition, we report a decrease in tumor latency indicating an early effect of the circadian disruption protocol over the progression of the disease.

Our main hypothesis was that desynchronization of the immune response could be involved in increased tumor growth rate in mice maintained under a CJL schedule. In this context, we first analyzed immune variables under normal LD conditions and found a daily pattern in the percentage of M1 and M2 macrophages in the spleen and in the tumor, as well as a daily variation in cytokine levels in the tumor. Specifically, our results showing higher levels of cytokines during the day are in line with reports showing a higher activity of macrophages (phagocytosis and cytokine secretion in vitro) in this phase of the LD cycle (*13*, *14*). Circadian regulation of macrophage function is also evidenced by the loss of rhythmic patterns in these cells in macrophage-specific $Bmal1^{-/-}$ mice (*15*). Overall, these data show not only that the macrophages have an internal clock but also that the clock is synchronized differentially depending on the tissue and functional profile.

Proinflammatory cytokines, mainly IL-1β and TNF-α, are usually associated with M1 macrophages (*27*). The apparent contradiction between the higher levels of these cytokines during the day and the higher percentage of M1 macrophages during the night in the tumor could be related to the presence of other cell types in this tissue, such as DC or T helper $CD4^+$, or with the time it takes macrophages to differentiate and synthesize these molecules. In addition, it is important to mention that the M2 macrophages may exhibit different profiles that are not fully characterized (generally known as M2a, M2b, M2c, and M2d) and that some of them can secrete proinflammatory cytokines (*28*).

We also report that the CJL schedule induces the loss or inversion of the daily immune patterns observed under LD conditions, both in the spleen and in the tumor. In rats carrying tumors, NK cells from the spleen showed higher nocturnal levels of granzyme B, perforin, and interferon-γ, which were lost under a CJL schedule (*6*). Similarly, changes in the immune microenvironment inside the tumor, particularly in macrophage and T helper lymphocyte profiles, have been recently reported in a different murine model of tumorigenesis subject to circadian deregulation (*29*). Together, these data suggest a strong effect of circadian desynchronization on the immune system. The M1/M2 ratio, which showed higher values during the night under LD conditions, decreased under the CJL schedule. This change suggests a functional defect in the immune system inside the tumor, because a decrease in the M1/M2 ratio has been associated with a worsening prognosis in tumors (*12*). In addition, the higher levels of leukocytes (total $CD45^+$ and LTh $CD4^+$) observed in the tumors of animals subjected to CJL could be related to the deregulation of macrophage LD patterns because of their main role as chemokine producers. Here, we show that the increase of total leukocytes is not due to an increase in the percentage of total macrophages, MDSCs, or T_{regs}. These results are in line with reports showing that immune infiltration of monocytes, DCs, and lymphocytes did not change after synchronizing tumor tissue with dexamethasone (*30*), all of which point to the need for a more thorough characterization of specific profiles of immune cells and secreted chemokines. For example, the recruitment of monocytes to inflammatory sites is mediated by the CCL2 ligand (also known as MCP-1), an important chemoattractant that is regulated in a diurnal fashion and secreted by macrophages, among other cells (*31*). It was shown that BMAL1 is necessary to generate the rhythmic oscillations in *Ccl2* expression via BMAL1/CLOCK binding to E-box motifs in the Ccl2's promoter and recruitment of members of the repressor complex polycomb repressive complex 2 (PRC2) (*31*). We previously showed that CCL2, which has a rhythmic mRNA expression in the SCN, is involved in circadian-immune bidirectional regulation (*32*). As a result, we could not rule out that the altered pattern of immune variables reported in the present work results from deregulation in the circadian expression of the CCL2 chemokine. For another chemokine pathway, the Cxcr2 inhibitor SB265610 was able to reverse JL-induced metastases and changes in immune cells (*29*). In this context, it has been reported that chronic circadian deregulation can modify both the endogenous clock and the immune phenotypes and functions of macrophages (*33*, *34*). One possible mechanism to explain the increased tumoral growth rate in mice under the CJL schedule could be that the macrophage internal clock is impaired or deregulated, as we have found in liver tissue. In turn, this would affect macrophage function and therefore modify the immune microenvironment.

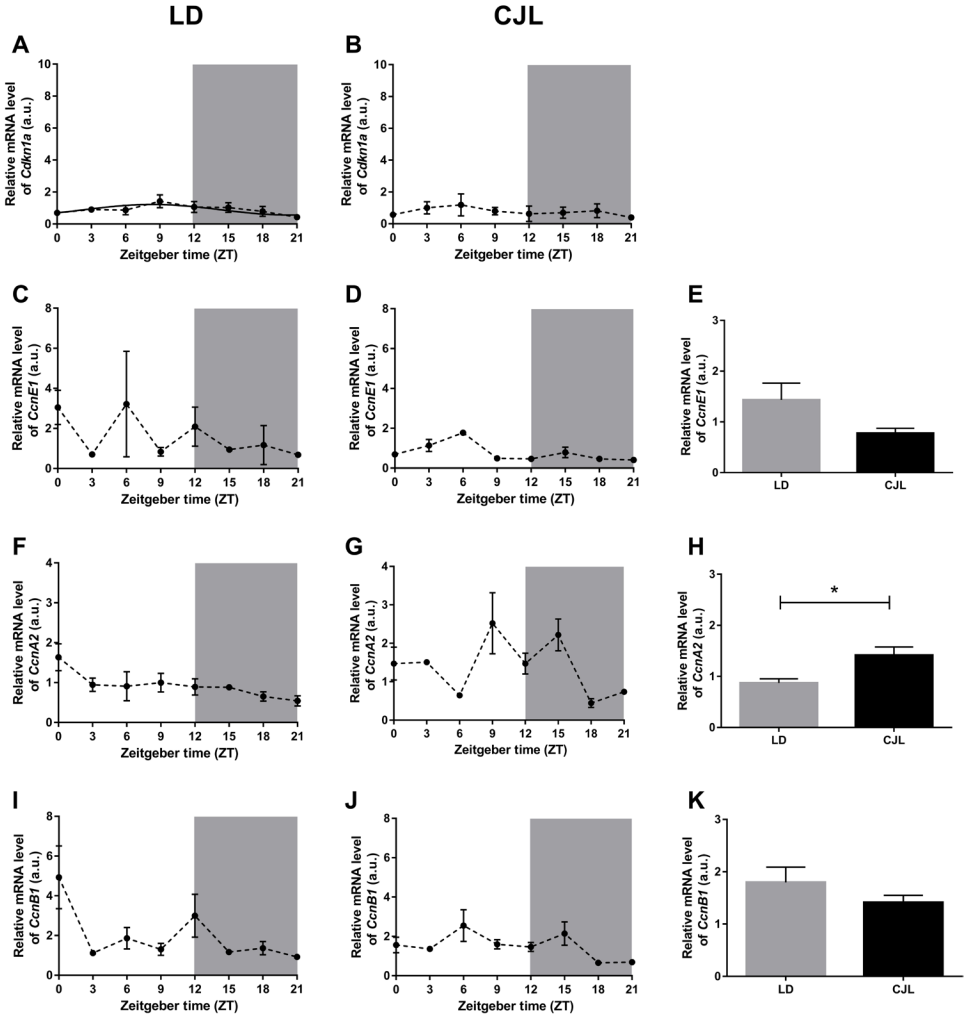

Fig. 6. Daily pattern of cell cycle–related molecules in tumor tissue under a CJL schedule. Mean ± SEM of relative mRNA levels of the inhibitor $p21^{WAF/CIP1}$ (*Cdkn1a*) (**A** and **B**), and *CcnE1* (**C** and **D**), *CcnA2* (**F** and **G**) and *CcnB1* (**I** and **J**) in tumor tissue of mice under LD (A, C, F, and I) and CJL (B, D, G, and J) conditions detected by real-time PCR at eight time points (ZT0, ZT3, ZT6, ZT9, ZT12, ZT15, ZT18, and ZT21), and mean ± SEM of 24-hour mean levels of *CcnE1* (**E**), *CcnA2* (**H**), and *CcnB1* (**K**). Curves plotted over the data (A) correspond to cosinor analysis adjusted to 24 hours. Only the statistically significant cosinor analyses were plotted. Student *t* test: $^*P < 0.05$; $n = 3$ to 4 per condition and time point.

As previously mentioned, chronic inflammation may be related to tumor progression. T helper 17 (T_H17) cells in some tumors act as promoters of chronic inflammation (*8*). However, in melanoma, these cells seem to be involved in the tumor regression process. In addition, the T_H17/T_{reg} rate inside the tumors is particularly relevant because they share differentiation pathways (*35*). Differentiation from $CD4^+$ naive T cells to a T_H17 profile is under circadian regulation through the inhibitory transcription factor NFIL3, which is regulated by Rev-erb-α. Accordingly, the T_H17 lineage is altered in Rev-erb-$\alpha^{-/-}$ mice. In addition, light cycle disruptions increased intestinal T_H17 cell frequencies and susceptibility to inflammatory disease (*36*). Furthermore, melatonin induces the expression of the repressor NFIL3, blocking differentiation to T_H17 cells and promoting the generation of T_{regs} and expression of IL-10 through induction by ROR-α (*37*). Deregulation in the T_H17 differentiation pathway induced by the CJL schedule may be related to the tendency to increase $CD4^+$ T_{regs} ($FoxP3^+$) in the tumors reported in the present study.

The CJL schedule altered the rhythmic expression patterns of the clock genes *Bmal1* and *Cry1* in the liver of control animals. The analysis of the rhythms of clock gene expression in the liver is relevant because it has been related to hepatocarcinogenesis (*21*). In addition, a complete loss of circadian rhythms in clock gene expression in several tissues has been reported in animals maintained under different CJL schedules (*21*, *38*). In line with our results, analysis of the molecular clock in muscles and lungs demonstrated that CJL schedules that advance the LD cycle 6 hours every 4 days induce an advance in the phase of the rhythm when studied immediately after CJL (*39*). Similarly, clock gene expression is phase-shifted in the spleen of control rats under a 6-hour advance every 2 days (*6*). Likewise, a phase shift in clock gene expression in the liver has been reported in tumor-bearing mice maintained under different CJL schedules (*20*, *38*).

As previously mentioned, the CJL schedule used in this work induces an activity pattern that includes two components of activity rhythm with periods of about 21 and 24.7 hours. It is possible to

divide this pattern in four phases: two "aligned" (activity or rest for both components) and two "misaligned" (activity for one component and rest for the other, in both directions). Although there are no data on the phases in peripheral tissues, we might speculate that when the phases are aligned, the peripheral rhythms will be more similar to a normal LD cycle, and in the misaligned condition, these variables lose their daily differences.

A potential confounding factor for the effect of circadian disruption is the lack of information about the "internal time" of the mice at the moment of the inoculation of tumor cells. The relative meaning of the different body rhythms (e.g., activity rhythms, temperature rhythms, and hormone rhythms) in this specific context is not yet fully understood. We established a 2-hour window for inoculation (ZT9 to ZT11) on the day following the 12-hour night of the CJL schedule. Moreover, because tumor development occurred throughout several desynchronization events (eight phase shifts per week), we could speculate that the differential tumoral growth depended on the complete schedule of disruption (30 to 45 days) and not necessarily on the time of inoculation. While we interpreted that the CJL protocol could affect the proliferation rate of the tumor cells and/or the antitumoral immune response, the circadian timing of inoculation could also modify the percentage of mice that developed tumors (a variable frequently reported in the existing literature), because the immune defense mechanisms would be different throughout the day.

Circadian regulation of the expression and activity of cell cycle–related molecules has been reported extensively, and circadian rhythms have been observed in the levels of c-Myc; cyclins E, A, B1, and D1; and the inhibitors Wee1, p16, p21, and p53, among others, in different systems [reviewed in (*40*, *41*)]. In addition, the distribution of the phases of the cell cycle (G_1-S-G_2) and the expression levels of molecules involved in apoptosis exhibit circadian rhythms in the bone marrow of mice (*42*). Here, we show that the daily expression pattern of cell cycle–related molecules observed under LD conditions was modified in the liver of mice maintained under the CJL schedule. In particular, the mRNA levels of the inhibitor $p21^{WAF/CIP1}$ lost their rhythmic expression patterns, while *CcnE1* rhythms were dampened. In line with our results, it was reported that the circadian expression of the proto-oncogene c-Myc, the cyclin D1, and the tumor suppressor Gadd45 was modified in the liver of *Per2* mutant mice (*43*), with an increase of c-Myc levels, a decrease of Gadd45 levels, and a phase shift of the circadian expression pattern of cyclin D1. Moreover, circadian clock disruption induced by a CJL schedule down-regulates p53 and up-regulates c-Myc levels in the liver of mice (*44*). Furthermore, chronic circadian desynchronization induces multiple oncogenic pathways to promote cell proliferation, thereby favoring G_1-S phase cell cycle progression (*45*). In addition, using a model of liver regeneration in mice, it has been shown that the circadian clock modulates the expression of cyclin B1, Cdc2 kinase, and wee1 (*46*). In particular, *wee1* could be transcriptionally regulated by Bmal1/Clock through the E-box sequences present in its promoter region. Here, we explored the mRNA levels of cell cycle–related molecules, but not their protein products, their activation levels, or the cell cycle phases; however, our results suggest an important deregulation of cell cycle–related transcription induced by circadian desynchronization.

As we previously mentioned, the night-day crepuscular peak of $p21^{WAF/CIP1}$ in the liver was lost in desynchronized animals, exhibiting low levels throughout the day. Similar LD patterns were reported in liver, heart, and skeletal muscle (*47*). In addition, the liver expression of $p21^{WAF/CIP1}$ was increased in Bmal1-deficient mice (*47*). However, as the $p21^{WAF/CIP1}$ promoter lacks E-box sequences, it is unlikely to be regulated directly by Bmal1/Clock. The expression of this molecule is regulated by Rev-erb-α (inhibitor) and ROR-α/ROR-γ (stimulator) through the RORE sequences present in its promoter region (*46*). Moreover, it is interesting that, in line with our observation about p21, circadian patterns of p53 in the thymus also became arrhythmic under a CJL schedule (*22*). On the other hand, an increased rate of cell division in the liver of mice maintained under a CJL schedule has been reported and was associated with the development of nonalcoholic fatty liver disease and hepatocarcinogenesis (*21*). This fact could be related to the decreased levels of the mentioned inhibitors p21 and p53.

In tumor tissue, we did not observe any rhythmic pattern in the mRNA levels of clock genes or cyclins. Similar results were recently published using the same tumor model (*30*). It is interesting that the intratumoral injection of dexamethasone in mice under an LD schedule not only reduced tumor growth rate but also induced the rhythmic expression of clock genes and a rhythmic pattern of mitosis and apoptosis in B16 melanoma tumors. These data show the relevance of studying (and inducing) rhythmic patterns inside the tumors.

However, it is important to emphasize that we measured the mRNA levels from a whole tumor tissue's fragment but did not evaluate the single-cell clock function. In this context, it is possible that each tumor cell maintains their rhythmic, cell-autonomous clock gene expression, but it is not identified because each cell exhibits a different circadian phase and the individual levels of these genes were compensated and, thus, invariant in the whole tissue extract. On the other hand, it is also possible that the circadian disruption observed in immune cell patterns inside the tumor affects the clock gene expression in the tumor cells through the secreted cytokines, because it has been reported that these molecules (e.g., TNF-α, IL-1, and CCL2) can modulate the molecular clock mechanism both in vitro and in vivo (*32*, *48*).

On the other hand, we observed that the levels of *CcnA2* were increased under CJL conditions. Despite the circadian expression of clock genes in several tumor cell lines in vitro, clock gene expression is generally impaired in most human cancers (*40*). Moreover, the number of rhythmic genes is reduced in human cancer samples and in immortalized cell lines compared to normal tissues (*40*). In addition, c-Myc levels inversely correlated with Bmal1, Clock, and Cry1/2 levels in human lymphomas. C-Myc is a transcription factor that binds the genome through E-boxes, the same binding sites of the Bmal1/Clock heterodimer. It has been reported that c-Myc inhibits clock gene expression in U2OS cells (*49*). Together, these data indicate a direct relationship between circadian and cell cycle–related molecules inside the tumors, which suggests that in our CJL model, deregulation of clock genes is part of the mechanism that affects tumoral transcription and activity.

In conclusion, our results suggest that circadian disruption could facilitate tumoral growth by modulating immune response and cell cycle–regulated factors. Specifically, we demonstrated that the circadian pattern of the immune response in the spleen and in the tumor, particularly in the percentage of pro- and anti-inflammatory macrophages, is deregulated under circadian desynchronization. The decrease in the M1 cells (and M1/M2 ratio) observed under CJL would tilt the balance toward a more tolerogenic immune profile,

which promotes tumor escape and tumoral progression. The peripheral immune desynchronization observed in the spleen of control animals maintained under the CJL schedule could affect the early stages of tumor development. In addition, animals subjected to a CJL schedule exhibited perturbations at the cellular level, which seems to make the liver cells competent to mitogenic signals. Our data suggest that desynchronization of the daily patterns of proinflammatory cytokines could favor cells becoming competent to mitogenic signals.

MATERIALS AND METHODS

Animals

Adult (2-month-old) C57BL/6J wild-type (WT) male mice (*Mus musculus*) were raised in our colony. Mice were housed under a 12:12-hour LD photoperiod (with lights on at 7:00 a.m. and lights off at 7:00 p.m.) with food and water ad libitum for at least 2 weeks before entering into experimental conditions. All animal protocols were approved by the Ethics Committee of the National University of Quilmes, and experiments were carried out in accordance with international ethical standards for the care and use of laboratory animals.

Cell culture

The mouse melanoma cell line B16F0, from D. F. Alonso from the Oncology Laboratory of the National University of Quilmes, was cultured in complete Dulbecco's modified Eagle's medium (Thermo Fisher Scientific) supplemented with 5% (v/v) fetal bovine serum (FBS) and maintained at 37°C in a humidified incubator with 5% CO_2.

Experimental lighting schedules

Individually caged animals (C57BL/6J, males, 2 to 3 months old) were maintained for 3 weeks under light:dark (LD12:12) or CJL [6-hour advance of the LD12:12 cycle every 2 days, shortening of every second dark phase (*9*)] schedules with food and water ad libitum. ZT was used as a temporal reference: ZT0 is the moment of lights on, and ZT12 is the moment of lights off. For the CJL schedule, samples were taken during the 12-hour night and on the following day. Effective circadian desynchronization was confirmed by individually monitoring locomotor activity rhythms using infrared sensors connected to a computer interface and by recording activity counts every 5 min. Data collection was used for posterior time series analysis (Archron, Buenos Aires, Argentina). In all cases, CJL-treated animals were confirmed for the presence of two components of activity rhythms with periods of ~21 and 24.7 hours as previously described (*9*).

In vivo experimental design

Mice were housed under either an LD or CJL schedule for 3 weeks before being inoculated with B16F0 cells or vehicle and maintained under the corresponding light schedule throughout the experimental procedure (until the end point of the tumorigenic protocol). To induce tumorigenesis, 30,000 cells were inoculated subcutaneously in the dorsal cephalad site of mice. Injections of all animals were carried out during a 2-hour window, ZT9 to ZT11, a time frame at which the day (which followed a 12-hour night) in CJL overlapped with that of the LD animals. Animals were manually palpated three times a week, and the day of tumor detection was recorded (latency to approximately 1 mm^3). From then on, the tumor size was measured with a caliper three times a week. The experimental end point was defined by the size of the tumor (2000 to 2500 mm^3 of volume) and in accordance with the Ethics Committee and Institutional Animal Care and Use guidelines of the National University of Quilmes. Animals were sacrificed at various ZTs (ZT0, ZT3, ZT6, ZT9, ZT12, ZT15, ZT18, and ZT21) when tumors reached the end point; this was in experiments that involved monitoring tumor growth, survival, and number of blood vessels. In cases where tissue gene expression and the immune makeup were monitored, samples were collected when tumors were of 1000 to 1500 mm^3 volume.

Quantification of blood vessels in tumor samples

Tumor samples were excised, fixed in 4% paraformaldehyde, embedded in paraffin, and stained using the hematoxylin and eosin method. Images (10 frames) were taken for the different tumor sections. Stained endothelial cells were visually identified and counted as surrounding blood vessel cells.

Neoangiogenesis

To determine neoangiogenesis, animals were intradermally coinjected with either B16F0 cells (100,000) or vehicle and trypan blue (0.2%) and sacrificed 7 days later. Blood vessel bifurcations were counted on the open skin. For accurate measurements, a 1.5-cm ruler was placed by the injection spot and pictures were taken. Blood vessel bifurcations were counted using ImageJ software (National Institutes of Health, Maryland, USA; https://imagej.nih.gov/ij/).

RNA extraction and real-time PCR

Liver and tumor tissues were carefully dissected from mice exposed to CJL or LD conditions. Total RNA was isolated using 300 μl of TRIzol reagent (Life Technologies) according to the manufacturer's instructions. RNA solutions were quantified using NanoDrop1000 (Thermo Fisher Scientific), and their integrity was evaluated by electrophoresis. One microgram of total RNA was treated with RQ1 RNase-Free DNase (Promega), and complementary DNA (cDNA) was synthesized using oligo(dT) primers and the SuperScript First-Strand Synthesis System (Invitrogen). Gene amplification was performed on a StepOne Plus Real-Time PCR instrument (Applied Biosystems), using 10 μl of final reaction volume containing 0.5 μl of cDNA as the template, 1× of the PerfeCTa FastMix II ROX (Quantabio, 95119-2), and the corresponding primers (table S3) at a final concentration of 200 to 400 nM. The cDNA template was amplified in triplicate, with the following conditions: 95°C for 2 min, followed by 40 cycles of 95°C for 15 s and 60°C for 1 min. Relative gene expression was calculated using the $2^{-\Delta\Delta Ct}$ method, and *hprt* was the reference housekeeping gene.

Flow cytometry

Tumor and spleen tissues were collected in culture medium containing collagenase IV (1 mg/ml; Thermo Fisher Scientific). Following mechanical disruption, tissues were maintained at 37°C for 20 min before the collagenase activity was inhibited by adding 15% FBS. Next, cells were filtered with a 70-μm filter, and red cells were incubated with lysis buffer [NH_4Cl (8290 μg/ml), $KHCO_3$ (1 μg/ml), and EDTA 1 mM] in a 1:9 ratio and then centrifuged at 400*g* for 10 min at 4°C. About 1×10^6 cells were incubated with the indicated fluorescent antibody (CD45, F4/80, CD11b, CD86, CD4, CD206, and Gr1; BioLegend) or their corresponding isotype control [phycoerythrin (PE) immunoglobulin G1a (IgG2a), PE IgG2b, PerCP7cy5.5 rat IgG2a, allophycocyamin (APC) rat IgG2a; BioLegend] for 30 min at room temperature. Cells were then washed with 3% phosphate-buffered saline (PBS)–FBS, centrifuged at 400*g* for 10 min, and fixed.

CD4-labeled cells were fixed at 4°C for 30 min, permeabilized for 30 min at 37°C using the FoxP3 buffer set (BD Pharmingen), and incubated with anti-FoxP3 (BioLegend) for an additional 30 min at room temperature. Fluorescence detection was carried out using a FACSCalibur flow cytometer (Becton Dickinson). Data were analyzed using FlowJo 7.6 software (http://flowjo.com).

The leukocyte population ($CD45^+$) in tumor cell suspension was analyzed using a CD45 versus side-scattered dot plot, and the cell-specific markers were analyzed inside this gate (fig. S4). For M1 and M2 macrophage analysis, the $F4/80^+$ (macrophage marker) population was plotted for CD86 and CD206 markers, and $CD86^+CD206^-$ cells were considered M1 and $CD86^-CD206^+$ cells were considered M2 [similar percentage of $CD86^+CD206^+$ population was observed in all group of samples (*50*)]. In addition, the M1/M2 ratio was calculated in each sample. MDSCs were identified as $CD11b^+Gr1^+$ and T_{reg} as $CD4^+FoxP3^+$. A similar procedure was followed to identify the spleen immune populations.

Cytokine detection in tissues

Tumor tissues from samples taken at ZT6 and ZT18 (day and night, respectively) were homogenized in PBS buffer containing a protease inhibitor cocktail (Sigma-Aldrich), incubated for 15 min at 4°C, and centrifuged at 14,000*g* for 15 min. Supernatants were collected, and protein concentration was measured using the Qubit Kit (Invitrogen). Concentration of cytokines TNF-α, IL-6, and IL-1β was determined by enzyme-linked immunosorbent assay (ELISA; Becton Dickinson Company) following the manufacturer's protocol.

Statistical analysis

Data are presented as mean ± SEM. Differences between two groups were analyzed using the unpaired Student's *t* test. Differences between more than two groups were analyzed by one- or two-way ANOVA or the nonparametric Kruskal-Wallis test. The *P* values of 0.05 or less were considered to be statistically significant. GraphPad Prism7 (GraphPad Software Inc.) and Infostat software were used to perform all statistical analyses. El Temps software was used for chronobiological analyses.

The two-way ANOVA was used to evaluate immunological parameter with the following factors being considered: time of sample extraction (day versus night), light schedule (LD versus CJL), and their interaction time × light schedule. The Kruskal-Wallis test was used to evaluate differences in gene expression among time points as experientially determined by real-time PCR. Cosinor analysis was additionally applied for the expression patterns that adjusted to cosenoidal curves with a period of 24 hours. Values of amplitude, acrophase, and mesor of the significant cosinor adjustments were used to plot the corresponding curves over the data. In expression patterns without any significant difference between time points (Kruskal-Wallis test and cosinor analyses), the 24-hour mean levels were calculated by gathering the values obtained in all samples.

Chi-square periodograms were performed to confirm circadian desynchronization in CJL maintained mice. As expected (*9*), in all cases, we observed two rhythmic components with periods around 21 and 24.7 hours.

SUPPLEMENTARY MATERIALS

Supplementary material for this article is available at http://advances.sciencemag.org/cgi/content/full/6/42/eaaz4530/DC1

View/request a protocol for this paper from *Bio-protocol*.

REFERENCES AND NOTES

1. Z. Chen, S. H. Yoo, J. S. Takahashi, Development and therapeutic potential of small-molecule modulators of circadian systems. *Annu. Rev. Pharmacol. Toxicol.* **58**, 231–252 (2018).
2. J. A. Mohawk, C. B. Green, J. S. Takahashi, Central and peripheral circadian clocks in mammals. *Annu. Rev. Neurosci.* **35**, 445–462 (2012).
3. D. A. Golombek, L. P. Casiraghi, P. V. Agostino, N. Paladino, J. M. Duhart, S. A. Plano, J. J. Chiesa, The times they're a-changing: Effects of circadian desynchronization on physiology and disease. *J. Physiol. Paris* **107**, 310–322 (2013).
4. J. S. Takahashi, Transcriptional architecture of the mammalian circadian clock. *Nat. Rev. Genet.* **18**, 164–179 (2017).
5. N. Cermakian, T. Lange, D. Golombek, D. Sarkar, A. Nakao, S. Shibata, G. Mazzoccoli, Crosstalk between the circadian clock circuitry and the immune system. *Chronobiol. Int.* **30**, 870–888 (2013).
6. R. W. Logan, C. Zhang, S. Murugan, S. O'Connell, D. Levitt, A. M. Rosenwasser, D. K. Sarkar, Chronic shift-lag alters the circadian clock of NK cells and promotes lung cancer growth in rats. *J. Immunol.* **188**, 2583–2591 (2012).
7. T. Chanmee, P. Ontong, K. Konno, N. Itano, Tumor-associated macrophages as major players in the tumor microenvironment. *Cancer* **6**, 1670–1690 (2014).
8. S. Shalapour, M. Karin, Immunity, inflammation, and cancer: An eternal fight between good and evil. *J. Clin. Invest.* **125**, 3347–3355 (2015).
9. L. P. Casiraghi, G. A. Oda, J. J. Chiesa, W. O. Friesen, D. A. Golombek, Forced desynchronization of activity rhythms in a model of chronic jet lag in mice. *J. Biol. Rhythm.* **27**, 59–69 (2012).
10. R. B. Holmgaard, D. Zamarin, Y. Li, B. Gasmi, D. H. Munn, J. P. Allison, T. Merghoub, J. D. Wolchok, Tumor-expressed IDO recruits and activates MDSCs in a T_{reg}-dependent manner. *Cell Rep.* **13**, 412–424 (2015).
11. M. Binnewies, E. W. Roberts, K. Kersten, V. Chan, D. F. Fearon, M. Merad, L. M. Coussens, D. I. Gabrilovich, S. Ostrand-Rosenberg, C. C. Hedrick, R. H. Vonderheide, M. J. Pittet, R. K. Jain, W. Zou, T. K. Howcroft, E. C. Woodhouse, R. A. Weinberg, M. F. Krummel, Understanding the tumor immune microenvironment (TIME) for effective therapy. *Nat. Med.* **24**, 541–550 (2018).
12. M. Zhang, Y. He, X. Sun, Q. Li, W. Wang, A. Zhao, W. Di, A high M1/M2 ratio of tumor-associated macrophages is associated with extended survival in ovarian cancer patients. *J. Ovarian Res.* **7**, 19 (2014).
13. M. Hayashi, S. Shimba, M. Tezuka, Characterization of the molecular clock in mouse peritoneal macrophages. *Biol. Pharm. Bull.* **30**, 621–626 (2007).
14. M. Keller, J. Mazuch, U. Abraham, G. D. Eom, E. D. Herzog, H. D. Volk, A. Kramer, B. Maier, A circadian clock in macrophages controls inflammatory immune responses. *Proc. Natl. Acad. Sci. U.S.A.* **106**, 21407–21412 (2009).
15. J. E. Gibbs, J. Blaikley, S. Beesley, L. Matthews, K. D. Simpson, S. H. Boyce, S. N. Farrow, K. J. Else, D. Singh, D. W. Ray, A. S. Loudon, The nuclear receptor REV-ERBalpha mediates circadian regulation of innate immunity through selective regulation of inflammatory cytokines. *Proc. Natl. Acad. Sci. U.S.A.* **109**, 582–587 (2012).
16. F. Hatanaka, C. Matsubara, J. Myung, T. Yoritaka, N. Kamimura, S. Tsutsumi, A. Kanai, Y. Suzuki, P. Sassone-Corsi, H. Aburatani, S. Sugano, T. Takumi, Genome-wide profiling of the core clock protein BMAL1 targets reveals a strict relationship with metabolism. *Mol. Cell. Biol.* **30**, 5636–5648 (2010).
17. A. Corlu, P. Loyer, Regulation of the g1/s transition in hepatocytes: Involvement of the cyclin-dependent kinase cdk1 in the DNA replication. *Int. J. Hepatol.* **2012**, 689324 (2012).
18. N. Fausto, Liver regeneration. *J. Hepatol.* **32**, 19–31 (2000).
19. M. Wu, J. Zeng, Y. Chen, Z. Zeng, J. Zhang, Y. Cai, Y. Ye, L. Fu, L. Xian, Z. Chen, Experimental chronic jet lag promotes growth and lung metastasis of Lewis lung carcinoma in C57BL/6 mice. *Oncol. Rep.* **27**, 1417–1428 (2012).
20. E. Filipski, F. Delaunay, V. M. King, M. W. Wu, B. Claustrat, A. Grechez-Cassiau, C. Guettier, M. H. Hastings, L. Francis, Effects of chronic jet lag on tumor progression in mice. *Cancer Res.* **64**, 7879–7885 (2004).
21. N. M. Kettner, H. Voicu, M. J. Finegold, C. Coarfa, A. Sreekumar, N. Putluri, C. A. Katchy, C. Lee, D. D. Moore, L. Fu, Circadian homeostasis of liver metabolism suppresses hepatocarcinogenesis. *Cancer Cell* **30**, 909–924 (2016).
22. S. Lee, L. A. Donehower, A. J. Herron, D. D. Moore, L. Fu, Disrupting circadian homeostasis of sympathetic signaling promotes tumor development in mice. *PLOS ONE* **5**, e10995 (2010).
23. N. N. Guerrero-Vargas, R. Navarro-Espindola, M. A. Guzman-Ruiz, M. D. C. Basualdo, E. Espitia-Bautista, A. Lopez-Bago, R. Lascurain, C. Cordoba-Manilla, R. M. Buijs, C. Escobar, Circadian disruption promotes tumor growth by anabolic host metabolism; experimental evidence in a rat model. *BMC Cancer* **17**, 625 (2017).
24. Y. Yasuniwa, H. Izumi, K. Y. Wang, S. Shimajiri, Y. Sasaguri, K. Kawai, H. Kasai, T. Shimada, K. Miyake, E. Kashiwagi, G. Hirano, A. Kidani, M. Akiyama, B. Han, Y. Wu, I. Ieiri, S. Higuchi, K. Kohno, Circadian disruption accelerates tumor growth and angio/stromagenesis through a Wnt signaling pathway. *PLOS ONE* **5**, e15330 (2010).

25. M. Kim, K. T. Lee, H. R. Jang, J. H. Kim, S. M. Noh, K. S. Song, J. S. Cho, H. Y. Jeong, S. Y. Kim, H. S. Yoo, Y. S. Kim, Epigenetic down-regulation and suppressive role of DCBLD2 in gastric cancer cell proliferation and invasion. *Mol. Cancer Res.* **6**, 222–230 (2008).
26. E. Filipski, V. M. King, X. Li, T. G. Granda, M. C. Mormont, X. Liu, B. Claustrat, M. H. Hastings, F. Levi, Host circadian clock as a control point in tumor progression. *J. Natl. Cancer Inst.* **94**, 690–697 (2002).
27. S. R. Nielsen, M. C. Schmid, Macrophages as key drivers of cancer progression and metastasis. *Mediat. Inflamm.* **2017**, 9624760 (2017).
28. F. O. Martinez, S. Gordon, The M1 and M2 paradigm of macrophage activation: Time for reassessment. *F1000prime Rep.* **6**, 13 (2014).
29. E. Hadadi, W. Taylor, X. M. Li, Y. Aslan, M. Villote, J. Riviere, G. Duvallet, C. Auriau, S. Dulong, I. Raymond-Letron, S. Provot, A. Bennaceur-Griscelli, H. Acloque, Chronic circadian disruption modulates breast cancer stemness and immune microenvironment to drive metastasis in mice. *Nat. Commun.* **11**, 3193 (2020).
30. S. Kiessling, L. Beaulieu-Laroche, I. D. Blum, D. Landgraf, D. K. Welsh, K. F. Storch, N. Labrecque, N. Cermakian, Enhancing circadian clock function in cancer cells inhibits tumor growth. *BMC Biol.* **15**, 13 (2017).
31. K. D. Nguyen, S. J. Fentress, Y. Qiu, K. Yun, J. S. Cox, A. Chawla, Circadian gene Bmal1 regulates diurnal oscillations of Ly6C(hi) inflammatory monocytes. *Science* **341**, 1483–1488 (2013).
32. J. M. Duhart, L. Brocardo, M. L. Mul Fedele, A. Guglielmotti, D. A. Golombek, CCL2 mediates the circadian response to low dose endotoxin. *Neuropharmacology* **108**, 373–381 (2016).
33. O. Castanon-Cervantes, M. Wu, J. C. Ehlen, K. Paul, K. L. Gamble, R. L. Johnson, R. C. Besing, M. Menaker, A. T. Gewirtz, A. J. Davidson, Dysregulation of inflammatory responses by chronic circadian disruption. *J. Immunol.* **185**, 5796–5805 (2010).
34. S.-M. Kim, N. Neuendorff, R. C. Alaniz, Y. Sun, R. S. Chapkin, D. J. Earnest, Shift work cycle-induced alterations of circadian rhythms potentiate the effects of high-fat diet on inflammation and metabolism. *FASEB J.* **32**, 3085–3095 (2018).
35. I. I. Ivanov, L. Zhou, D. R. Littman, Transcriptional regulation of Th17 cell differentiation. *Semin. Immunol.* **19**, 409–417 (2007).
36. X. Yu, D. Rollins, K. A. Ruhn, J. J. Stubblefield, C. B. Green, M. Kashiwada, P. B. Rothman, J. S. Takahashi, L. V. Hooper, T_H17 cell differentiation is regulated by the circadian clock. *Science* **342**, 727–730 (2013).
37. M. F. Farez, I. D. Mascanfroni, S. P. Mendez-Huergo, A. Yeste, G. Murugaiyan, L. P. Garo, M. E. Balbuena Aguirre, B. Patel, M. C. Ysrraelit, C. Zhu, V. K. Kuchroo, G. A. Rabinovich, F. J. Quintana, J. Correale, Melatonin contributes to the seasonality of multiple sclerosis relapses. *Cell* **162**, 1338–1352 (2015).
38. E. Filipski, P. F. Innominato, M. Wu, X. M. Li, S. Iacobelli, L.-J. Xian, F. Levi, Effects of light and food schedules on liver and tumor molecular clocks in mice. *J. Natl. Cancer Inst.* **97**, 507–517 (2005).
39. G. Wolff, M. J. Duncan, K. A. Esser, Chronic phase advance alters circadian physiological rhythms and peripheral molecular clocks. *J. Appl. Physiol.* **115**, 373–382 (2013).
40. T. Matsu-Ura, S. R. Moore, C. I. Hong, WNT takes two to tango: Molecular links between the circadian clock and the cell cycle in adult stem cells. *J. Biol. Rhythm.* **33**, 5–14 (2018).
41. S. Masri, M. Cervantes, P. Sassone-Corsi, The circadian clock and cell cycle: Interconnected biological circuits. *Curr. Opin. Cell Biol.* **25**, 730–734 (2013).
42. T. G. Granda, X. H. Liu, R. Smaaland, N. Cermakian, E. Filipski, P. Sassone-Corsi, F. Levi, Circadian regulation of cell cycle and apoptosis proteins in mouse bone marrow and tumor. *FASEB J.* **19**, 304–306 (2005).
43. L. Fu, H. Pelicano, J. Liu, P. Huang, C. Lee, The circadian gene Period2 plays an important role in tumor suppression and DNA damage response in vivo. *Cell* **111**, 41–50 (2002).
44. A. Iwamoto, M. Kawai, M. Furuse, S. Yasuo, Effects of chronic jet lag on the central and peripheral circadian clocks in CBA/N mice. *Chronobiol. Int.* **31**, 189–198 (2014).
45. Y. Lee, N. F. Lahens, S. Zhang, J. Bedont, J. M. Field, A. Sehgal, G1/S cell cycle regulators mediate effects of circadian dysregulation on tumor growth and provide targets for timed anticancer treatment. *PLOS Biol.* **17**, e3000228 (2019).
46. T. Matsuo, S. Yamaguchi, S. Mitsui, A. Emi, F. Shimoda, H. Okamura, Control mechanism of the circadian clock for timing of cell division in vivo. *Science* **302**, 255–259 (2003).
47. A. Grechez-Cassiau, B. Rayet, F. Guillaumond, M. Teboul, F. Delaunay, The circadian clock component BMAL1 is a critical regulator of p21WAF1/CIP1 expression and hepatocyte proliferation. *J. Biol. Chem.* **283**, 4535–4542 (2008).
48. J. M. Duhart, M. J. Leone, N. Paladino, J. A. Evans, O. Castanon-Cervantes, A. J. Davidson, D. A. Golombek, Suprachiasmatic astrocytes modulate the circadian clock in response to TNF-alpha. *J. Immunol.* **191**, 4656–4664 (2013).
49. A. Shostak, B. Ruppert, N. Ha, P. Bruns, U. H. Toprak, R. Eils, M. Schlesner, A. Diernfellner, M. Brunner, MYC/MIZ1-dependent gene repression inversely coordinates the circadian clock with cell cycle and proliferation. *Nat. Commun.* **7**, 11807 (2016).
50. A. Vilaseca, N. Campillo, M. Torres, M. Musquera, D. Gozal, J. M. Montserrat, A. Alcaraz, K. A. Touijer, R. Farre, I. Almendros, Intermittent hypoxia increases kidney tumor vascularization in a murine model of sleep apnea. *PLOS ONE* **12**, e0179444 (2017).

Acknowledgments: We thank J. Webster for comments and manuscript editing. We also thank L. Trebucq and S. Plano for collaboration in sample collection. **Funding:** This work was supported by grants from the National Research Council (CONICET), the National Science Agency (ANPCyT), and the National University of Quilmes (UNQ) to D.A.G. and the National Science Foundation (NSF MCB-1517298) to C.V.F. **Author contributions:** I.A., M.L.M.F., and F.R. performed research and analyzed data; C.C. performed research; L.M. and J.J.C. contributed to the design of the study and performed the research; D.A.G., C.V.F., and N.P. conceived and designed the study and wrote the paper. **Competing interests:** The authors declare that they have no competing interests. **Data and materials availability:** All data needed to evaluate the conclusions in the paper are present in the paper and/or the Supplementary Materials. Additional data related to this paper may be requested from the authors.

Submitted 18 September 2019
Accepted 28 August 2020
Published 14 October 2020
10.1126/sciadv.aaz4530

Citation: I. Aiello, M. L. M. Fedele, F. Román, L. Marpegan, C. Caldart, J. J. Chiesa, D. A. Golombek, C. V. Finkielstein, N. Paladino, Circadian disruption promotes tumor-immune microenvironment remodeling favoring tumor cell proliferation. *Sci. Adv.* **6**, eaaz4530 (2020).

Circadian disruption promotes tumor-immune microenvironment remodeling favoring tumor cell proliferation

I. Aiello, M. L. Mul Fedele, F. Román, L. Marpegan, C. Caldart, J. J. Chiesa, D. A. Golombek, C. V. Finkielstein and N. Paladino

Sci Adv **6** (42), eaaz4530.
DOI: 10.1126/sciadv.aaz4530